Pharm Res (2012) 29:795–805
DOI 10.1007/s11095-011-0603-6

RESEARCH PAPER

Liver Cancer Targeting of Doxorubicin with Reduced Distribution to the Heart Using Hematoporphyrin-Modified Albumin Nanoparticles in Rats

Ji-Eun Chang • Won-Sik Shim • Su-Geun Yang • Eun-Young Kwak • Saeho Chong • Dae-Duk Kim • Suk-Jae Chung • Chang-Koo Shim

Received: 25 June 2011 / Accepted: 21 September 2011 / Published online: 5 October 2011

ABSTRACT

Purpose To evaluate the usefulness of hematoporphyrin (HP)-modification of the surface of doxorubicin (DOX)-loaded bovine serum albumin (BSA) nanoparticles (NPs) in the liver cancer-selective delivery of DOX.

Methods HP-modified NPs (HP-NPs) were prepared by conjugation of amino groups on the surface of NPs with HP, a ligand for low density lipoprotein (LDL) receptors on the hepatoma cells. *In vitro* cellular accumulation of DOX, *in vivo* biodistribution of DOX, safety, and anti-tumor efficacy were evaluated for HP-NPs.

Results Cytotoxicity and accumulation of DOX were in the order of HP-NPs>NPs>solution form (SOL). Cellular uptake from HP-NPs was proportional to the expression level of LDL receptors on the cells, indicating possible involvement of LDL receptor-mediated endocytosis (RME) in uptake. The "merit index," an AUC ratio of DOX in liver (target organ) to DOX in heart (major side effect organ) following iv administration of HP-NPs to hepatoma rats, was 132.5 and 4 times greater compared to SOL and NPs, respectively. The greatest suppression of body weight decrease and tumor size increase was observed for iv-administered HP-NPs in tumor-bearing mice.

Conclusions HP modification appears to be useful in selective delivery of NP-loaded DOX to tumors.

KEY WORDS doxorubicin · hematoporphyrin · liver cancer · nanoparticles · targeted delivery

ABBREVIATIONS

25-HC	25-hydroxycholesterol
BSA	bovine serum albumin
DOX	doxorubicin
HP	hematoporphyrin
HP-NP	hematoporphyrin-modified, doxorubicin-loaded nanoparticle
NP	doxorubicin-loaded nanoparticle
SOL	doxorubicin solution

INTRODUCTION

According to the 2011 American Cancer Society Data, liver cancer accounts for 4% of male and 2% of female cancer deaths, ranking 5th and 9th respectively compared to other cancers. Doxorubicin hydrochloride (DOX) is one of the most widely used antineoplastic agents, particularly for liver cancer (1,2), but unfortunately, it causes serious side effects such as irreversible cardiomyopathy and congestive heart failure (3). Side effects of cancer chemo-

J.-E. Chang • E.-Y. Kwak • C.-K. Shim (✉)
National Research Laboratory for Transporters Targeted Drug Design
Research Institute of Pharmaceutical Sciences
College of Pharmacy, Seoul National University
Seoul 151-742, South Korea
e-mail: shimck@snu.ac.kr

S. Chong • D.-D. Kim • S.-J. Chung
Research Institute of Pharmaceutical Sciences
College of Pharmacy, Seoul National University
Seoul 151-742, South Korea

W.-S. Shim
College of Pharmacy, Gachon University of Medicine and Science
Incheon 406-799, South Korea

S.-G. Yang
Department of Applied Bioscience, College of life science
CHA University
Gyeonggi-do 463-840, South Korea

therapy are generally associated with a substantial distribution of the drugs to normal tissues (4,5). A variety of permeation barriers on the cancer cell membranes limit the distribution of the drugs to the cells (6). Therefore, increasing the accumulation of anticancer drugs at tumor sites and decreasing the distribution to normal tissues would be highly desirable in the development of drug delivery systems.

To accomplish this, researchers have developed numerous targeted drug delivery systems using a variety of carriers including polymers, liposomes, microspheres, and nano-sized particles (7–9). The immature and porous vasculature of tumors may provide more opportunity for circulating particulate formulations to accumulate in tumors. For this reason, nanoparticles may be ideal drug carriers, since they are able to deliver loaded drugs selectively to tumors where particle size is a critical factor in uptake, i.e., passive targeting (10). For example, a pegylated liposomal formulation of doxorubicin (Doxil®) is currently used as an anti-cancer agent. However, even though albumin-bound paclitaxel nanoparticles (Abraxane™) are widely used for the treatment of breast cancer (11), it is generally believed that cancer-specific delivery is not sufficiently achievable solely by passive targeting approaches with standard nanoparticles, necessitating the functional modification of the nanoparticles. Modifying surface characteristics by introducing specific ligands for specific receptors on cancer-cell membranes is a frequently attempted approach (10,12).

Hematoporphyrin (HP) is a ligand that readily binds to low-density lipoprotein (LDL) receptors on tumor cell membranes (13). HP analogues, such as chlorin e6 and its PVP complex (Photolon™), are selectively accumulated in tumor tissues and are well known photosensitizers (14). Most importantly, improved targeting of ^{99m}Tc-labelled albumin nanoparticles to tumors has been achieved by the HP modification of nanoparticles (15). Albumin has been adopted in the design of various nanoparticles due to its biocompatibility (15).

In the present study, the surface of BSA nanoparticles containing DOX (NPs) was modified using HP to prepare HP-modified NPs (HP-NPs), and the effect of the modification on *in vitro* uptake into, and cytotoxicity against, HepG2 cells and on *in vivo* targeting of DOX to liver tumors following intravenous (iv) administration to liver cancer-induced rats was investigated. Of particular interest was the distribution of DOX to the liver (target organ) and heart (toxicity organ) in the *in vivo* study.

MATERIALS AND METHODS

Materials

Doxorubicin hydrochloride (DOX), bovine serum albumin (BSA, purity ≥98%), glutaraldehyde 8% solution, N-hydroxysuccinimide (NHS, 98%), 25-hydroxycholesterol (25-HC) and Dulbecco's Modified Eagle medium (DMEM) were purchased from Sigma-Aldrich Co. (St. Louis, MO, USA). Hematoporphyrin dihydrochloride (HP) was acquired from Tokyo Chemical Industry Co., Ltd. (Tokyo, Japan). N, N-dicyclohexylcarbodiimide (DCC, purity >99%) was obtained from Fluka (Tokyo, Japan). Fetal bovine serum (FBS) was purchased from Hyclone Laboratories (Logan, UT, USA). Solvents such as ethanol, dimethyl sulfoxide (DMSO), acetonitrile, and all other reagents were obtained from Fisher Scientific Korea Ltd. (Seoul, Korea).

Preparation of DOX-Loaded Nanoparticles (NPs)

NPs were prepared by a desolvation technique (16,17) with 10 mg of DOX and 200 mg of BSA dissolved in 10 mL of purified water. The solution was then stirred for 2 h at room temperature until the DOX was fully adsorbed by the BSA. Then 30 mL of ethanol was added at 1 mL/min using an infusion pump from KD Scientific (Holliston, MA, USA) under constant stirring at 300 rpm at room temperature. For the desolvation process, 8% glutaraldehyde solution (1.175 μL/mg BSA) was added as a cross-linking agent under constant stirring at 300 rpm for 24 h to stabilize the nanoparticles. The resulting nanoparticles, were purified by centrifugation (Centrifuge 5415R, Eppendorf AG Hamburg, Germany) at 16,000 × *g* for 12 min; then redispersion in double-distilled water (DDW) was repeated 3 times to eliminate the ethanol and glutaraldehyde. The supernatants were then collected to measure drug content and loading efficiency.

Conjugation of Hematoporphyrin (HP) to Prepare HP-Modified NPs (HP-NPs)

20 μmol of HP, 40 μmol of NHS, and 40 μmol of DCC were added to 2 mL of DMSO and stirred overnight in the dark at room temperature to prepare hematoporphyrin N-hydroxysuccinimide ester (HP-NHS) (16,18). The mixture was then filtered to remove insoluble dicyclohexylurea. HP-NHS was isolated by mixing the filtrate with excess diethyl ether under constant stirring at 300 rpm and washed with methanol. This step was repeated once. The sample was lyophilized and stored at −20°C. HP modification of NPs was performed using HP-NHS conjugation with an amide linkage (19). HP-NHS was dissolved in a 2.5% w/v aqueous suspension of NPs at a weight ratio of 1:4, and stirred overnight at 300 rpm at room temperature. Centrifugation at 16,000 × *g* for 12 min and redispersion in DDW were repeated 3 times to eliminate unreacted HP-NHS. The remaining unreacted amino groups of NPs were measured by trinitrobenzenesulfonic acid (TNBS) determination (20).

Size, Zeta Potential, and Morphology Determinations

The mean particle size and zeta potential of the nanoparticles (i.e., NPs and HP-NPs) were measured by dynamic light scattering using an electrophoretic light scattering spectrophotometer (ELS-8000, Otsuka Electronics Co. Ltd. Osaka, Japan). The samples were diluted with DDW to 0.1 mg/mL and measured at a wavelength of 633 nm at a fixed angle of 90° at 25°C (21).

The size and the morphology were then examined by field-emission scanning electron microscopy (FE-SEM) (SUPRA 55VP, Carl Zeiss, Oberkochen, Germany) and transmission electron microscopy (TEM) (JEM 1010, JEOL, Tokyo, Japan) (22). For the FE-SEM measurements, nanoparticles were dispersed in DDW, and the dispersions were dropped onto a carbon mount followed by drying in a vacuum chamber for 24 h at 25°C. For the TEM measurement, ultrasonic dispersions of powders in DDW were dropped onto a carbon-coated copper grid.

Loading Content and Loading Efficiency

The loaded content and loading efficiency of DOX in the nanoparticles (i.e., NPs and HP-NPs) were measured by high-performance liquid chromatography (HPLC). Nanoparticles were dissolved in the mobile phase, a mixture of acetonitrile and deionized water (35:65 by volume with pH adjusted to 2.4 by phosphoric acid and NaOH), and the aliquots were chromatographed for the assay of DOX using a 250 mm×4.6 mm C18 column (Varian, Inc., Santa Clara, CA, USA), which was protected by a guard column. The flow rate of the mobile phase was 1 mL/min, and the temperature was 30°C. The column effluent was monitored with a fluorescence detector (Jasco FP-2020 Plus, Tokyo, Japan) at wavelengths of 480 nm for excitation and 560 nm for emission. Daunorubicin was used as an internal standard (23). Loading content and loading efficiency were calculated by the following formulas (12).

$$\text{Loading content}(\%) = \frac{\text{weight of DOX in NPs}}{\text{weight of NPs}} \times 100$$

$$\text{Loading efficiency}(\%) = \frac{\text{weight of DOX in NPs}}{\text{weight of DOX added}} \times 100$$

In Vitro Release Study

The release of DOX from the nanoparticles (i.e., NPs and HP-NPs) was measured in a phosphate buffered saline (PBS) medium, with a pH of 7.4 by HPLC (24). 10 mg of nanoparticles was dispersed in 10 mL of PBS in Eppendorf tubes, and the tubes were placed in a water bath at 37°C and shaken continuously at 120 strokes/min. At specific time intervals, the tubes were centrifuged, and the supernatants were assayed for DOX using HPLC in the aforementioned procedure. The remaining pellets were resuspended in 10 mL of fresh PBS for continuous release study. This analysis was conducted on 3 samples each of NPs and HP-NPs.

Cell Viability Assay

The cytotoxicity of a PBS solution of DOX (SOL), NPs, and HP-NPs against human hepatocellular carcinoma HepG2 cells (ATCC, Manassas, VA, USA) was determined by MTT assay (25,26). The cells were seeded on 24-well plates at a density of 5×10^4 cells/well in DMEM medium containing 10% (v/v) FBS and 1% (w/v) penicillin-streptomycin and incubated overnight at 37°C in a humidified 5% CO_2 and 95% air atmosphere. The medium was washed off and replaced with new media containing SOL, NPs, or HP-NPs of various DOX concentrations (0.01–10 μM). After 48 h incubation, cells were washed twice with cold PBS to eliminate the remaining drugs. Subsequently, the cells were incubated for 4 h with 50 μL/well of medium containing 1 mg/mL of MTT agent, and 500 μL/well of DMSO was added. The plates were shaken gently, and absorbance was read at a wavelength of 540 nm using a multiwell scanning spectrophotometer (KC4, Bio-Tek Instruments, INC., Winooski, VT, USA). Cytotoxicity was expressed as the percentage of the control. The IC_{50} value was defined as the DOX concentration required to inhibit the growth by 50% as compared to DOX-unloaded nanoparticles. All the experiments were performed in triplicate.

Cellular Accumulation Study

HepG2 cells were seeded in 24-well plates with glass coverslips at a density of 1×10^5 cells/well. The cells were incubated with DMEM medium containing 10% FBS and 1% (w/v) penicillin-streptomycin for 1 day to allow cell attachment. On the following day, NPs, HP-NPs and free DOX in DMEM medium were added, respectively, at 170 μM as DOX concentration, and the cells were incubated for 6 h. A high concentration of DOX was adopted in the present study in order to clearly visualize the confocal images and to readily observe the FACS data. The 6 h of exposure time was appropriate to observe the uptake of DOX from the nanoparticles into HepG2 cells (27). The plates were washed 3 times with cold PBS and examined by confocal laser scanning microscopy at an excitation wavelength of 480 nm and an emission wavelength of 560 nm (CLSM, Carl Zeiss, LSM510, Gottingen, Germany) (28). The level of DOX in the cells was measured by flow cytometry (FACSCalibur, BD Biosciences, San Jose, CA,

USA) using CellQuest software (BD Immunocytometry Systems, Mountain View, CA, USA) (27).

The accumulation was also measured in 25-hydroxycholesterol (25-HC, Sigma, St. Louis, MO, USA)—pretreated HepG2 cells. HepG2 cells were seeded in 24-well plates for 1 day and pretreated with 0, 10, 100, and 1000 μg/mL of 25-HC for 48 h. Thereafter, cells were collected, and standard RT-PCR was performed with custom-designed oligomers (Forward: 5′-CTC GCT GGT GAC TGA AAA CA-3′, Reverse: 5′-CAA AGG AAG AG AGG AGC AC-3′) that specifically bind to human LDL receptor genes at 94°C for 4 min followed by 30 cycles of 94°C for 30 s, 55°C for 30 s, and 72°C for 30 s with an additional cycle of 72°C for 3 min to conclude the program. Amplicons were detected by gel electrophoresis, and glyceroaldehyde-3-phosphate dehydrogenase (GAPDH) was used as a control. For confocal microscopy, HepG2 cells were seeded in a similar manner. Cells were treated with 0, 10, 100, 1000 μg/mL 25-HC for 48 h, washed 3 times with cold PBS, and incubated with HP-NPs or NPs at 170 μM as DOX. Cells were washed 3 times with cold PBS, and the accumulation of DOX was determined by confocal laser scanning microscopy.

Tissue Distribution Study in Normal and Liver Cancer-Induced Rats

All animal study protocols were approved by the Animal Care and Use Committee of the College of Pharmacy, Seoul National University. Male Sprague-Dawley (SD) rats weighing 250–300 g were used (Orient Co., Institute, Kyungki-Do, Korea). The N1-S1 rat hepatoma cell line, which was kindly supplied by Inha University, was cultured in Iscove's Modified Dulbecco's Medium (Welgene, Inc., Daegu, Korea) containing 10% FBS and 1% (w/v) penicillin-streptomycin. The rats were anesthetized with ketamine (50 mg/kg, intramuscular injection), shaved, and the left and right lobes of the livers were exposed. 1×10^6 cells/0.5 mL of tumor cell suspension was slowly injected directly into each lobe using a 30-gauge needle, and the injection site was pressed with sterilizing gauze for 30 s to stop the bleeding. The wound was then closed with a surgical suture. Two weeks later (29,30), drugs were administered as follows.

Under the same anesthesia, normal and liver cancer-induced rats were cannulated with polyethylene tubing (PE-50, Intramedic, Clay Adams, Sparks, MD, USA) (31), and SOL and PBS dispersions of NPs and HP-NPs were injected into the left femoral veins of the rats at a DOX dose of 2 mg/kg body weight. At intervals of 1, 2, 4, 6, 12, 24, and 48 h after injection, the rats were euthanized, and their livers, hearts, spleens, lungs, kidneys, and brains were excised immediately thereafter. The tissues were quickly washed twice with cold normal saline, weighed, and homogenized with normal saline using a tissue homogenizer (Ultra-Turrax T25, IKA-Labortechnik, Staufen, Germany). 100 μL of homogenates were spiked with 50 μL of internal standard (daunorubicin, 2 μg/mL) and extracted with ethyl acetate and methanol. The extract was centrifuged at 16,000 × *g* for 3 min, and the supernatants were evaporated under nitrogen gas. The residue was dissolved in a mobile phase (a mixture of acetonitrile and deionized water, 35:65 by volume with pH adjusted to 2.4 by phosphoric acid and NaOH), and the fluorescence intensities were measured using an HPLC system as described above. The DOX concentration in the tissues was expressed as the amount of DOX per gram of tissue. The area under the tissue concentration of DOX for the measured period of 1–48 h (AUC) was calculated using a trapezoidal rule.

Safety and Anti-tumor Efficacy in Liver Cancer-Induced Mice

Mice were adopted in the present study because the tumor size could be measured only in mice. BALB/C male nude mice (6–7 weeks, 20–22 g) were purchased from Hanlim Experimental Animal Center (Kyungki-Do, Korea). 1×10^6 HepG2 cells in 0.1 mL DMEM medium were injected subcutaneously into the left flanks of the mice (10). When the mean tumor volume exceeded approximately 500 mm^3, which was 10 days after the injection, the safety and anti-tumor efficacy study was begun (day 0). The mice that had liver tumors were randomly divided into 4 groups ($n=5$ each) of PBS, SOL, NPs, and HP-NPs. Each formula was injected into the tail vein at a DOX dose of 2 mg/kg in PBS 4 times at 4-day intervals (i.e., days 0, 4, 8, and 12). The tumor size and body weight of each mouse was monitored for 3 weeks. Tumors were measured with a caliper, and the tumor volume was calculated using the following formula (32):

$$\text{Tumor volume}(mm^3) = (\text{length} \times \text{width}^2)/2.$$

Table I Particle Size, Zeta Potential, DOX-Loading Content, and DOX-Loading Efficiency of NPs and HP-NPs

Samples ($n=4$)	Particle size (nm)	Zeta potential (mV)	Loading content (%)	Loading efficiency (%)
NPs	341.6 ± 10.4	−28.4 ± 1.4	3.89 ± 1.1	58.1 ± 1.6
HP-NPs	372.6 ± 10.9*	−20.0 ± 1.6*	2.96 ± 1.0	50.8 ± 3.2*

* $p<0.05$

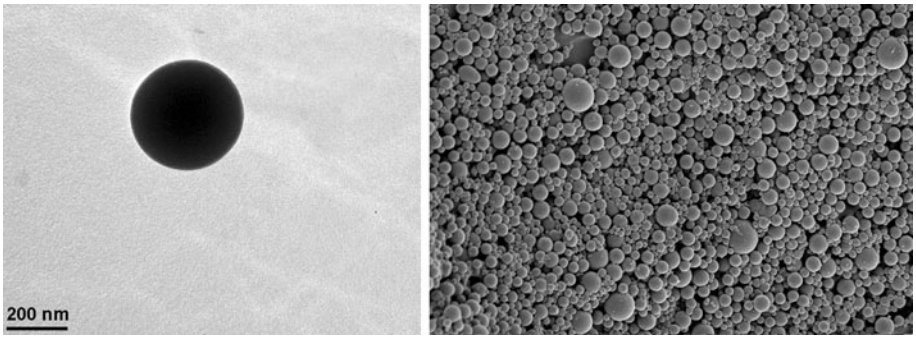

Fig. 1 Representative TEM (*left*) and FE-SEM (*right*) images of HP-NPs.

Statistical Analysis

All data were presented as the mean ± standard deviation. The statistical significance between the groups was determined by using the Student's *t*-test for 2 groups or one-way ANOVA with Tukey's *post-hoc* test for more than 3 groups. It was considered significant when p values were less than 0.05.

RESULTS

Physical Characteristics of NPs and HP-NPs

Some physical characteristics such as particle size, zeta potential, and loading efficiency were slightly, but significantly, changed by HP modification (Table I). According to the TNBS determination for HP-NPs, 60.2%±2.3% (n=4) of amino groups on the surface of NPs were cross-linked with HP, indicating successful modification of the NP surfaces with HP. TEM and FE-SEM (Fig. 1) showed a uniform, smooth and spherical shape for the HP-NPs without unloaded drug crystals on the surfaces.

In Vitro Release of DOX from NPs and HP-NPs

In vitro release profiles of DOX in PBS (pH 7.4) were not significantly different between NPs and HP-NPs. Both HP-NPs and NPs showed a burst release at the initial stage with approximately 23% of loaded DOX released within 4 h, and more than 50% of the drug released within 24 h. Sustained release for up to 160 h afterwards was observed.

In Vitro Potency of NPs and HP-NPs

After 48 h treatment in the MTT assay, all of the samples showed cytotoxicity, which was proportional to the applied DOX concentration. HP-NPs showed the strongest cytotoxicity among tested formulations for all DOX concentrations (Fig. 2). The IC_{50} of SOL, NPs, and HP-NPs against HepG2 cells, which means DOX concentrations that lead to 50% cell-killing, were 14.76, 1.32 and 0.67 μM, respectively. At 10 μM DOX concentration, for example, a dramatic decrease in cell viability was observed for HP-NPs (11.2±1.92, n=3) compared to NPs (27.74±1.47, n=3) and SOL (66.5±1.40, n=3) indicating the greatest cellular accumulation of DOX from HP-NPs. A greater potency of HP-NPs than NPs appeared to indicate greater cellular uptake of DOX from HP-NPs.

Cellular Accumulation of DOX from NPs and HP-NPs

After 6 h of treatment with nanoparticles, fluorescence intensity of the HepG2 cells was much stronger for HP-NPs (Fig. 3c) compared with NPs (Fig. 3b). A similar result was obtained from FACS analysis (Fig. 4). The cells treated with HP-NPs demonstrated much higher fluorescence intensity than the cells treated with NPs. These results indicate that cellular uptake of DOX was greatly enhanced by HP conjugation to NPs, supporting the results from the cell viability assay (Fig. 2).

Correlation of Accumulation with the Expression Level of LDL Receptors

Previous reports have claimed that HP enters the cell through an LDL receptor-mediated endocytosis mechanism (33). Since HP-NPs showed increased accumulation of DOX into HepG2 cells compared to NPs, the involvement

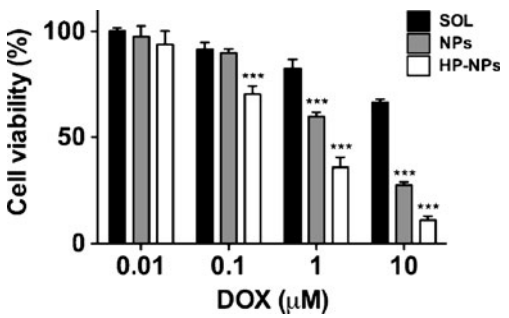

Fig. 2 The viability of human hepatocellular carcinoma HepG2 cells after 48 h treatment with SOL (*black*, n=3), NPs (*gray*, n=3) and HP-NPs (*white*, n=3) at 37°C. Each sample was measured using MTT assays. *** $p<0.001$, compared to SOL.

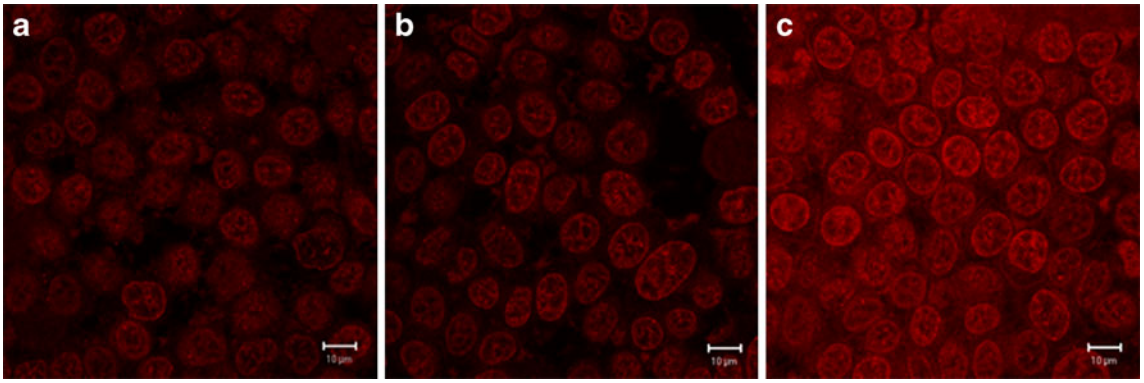

Fig. 3 Representative confocal images of HepG2 cells after treatments with SOL (**a**), NPs (**b**) and HP-NPs (**c**) at 37°C for 6 h at DOX concentration of 170 μM: red fluorescence corresponds to DOX in the cell.

of LDL receptors in the uptake of HP-NPs was tested. A strong band of LDL receptors was detected from the control cells indicating an abundance of these receptors in HepG2 cells. However, when 25-HC, a downregulator of LDL receptors (34), was treated, the band intensities of LDL receptors were significantly reduced with increased concentration of 25-HC, indicating significant down-regulation of the receptors in mRNA levels (Fig. 5).

Confocal microscopic studies revealed a significantly reduced cellular accumulation of DOX from HP-NPs after 25-HC pretreatment (Fig. 6a–d). On the other hand, no reduction caused by pretreatment was observed for the accumulation of DOX from NPs (Fig. 6e–h). The reduced accumulation for HP-NPs was parallel with the reduced expression of LDL receptors by 25-HC (Fig. 5). Therefore, it was suggested that the increased accumulation of DOX from HP-NPs was attributable to increased uptake of HP-NPs via LDL receptors on the cellular membrane.

Tissue Distribution of DOX from NPs and HP-NPs

Figures 7 and 8 represent temporal profiles of DOX in the liver, heart, spleen, lung, kidney, and brain for normal and hepatoma-induced rats, respectively, following iv administration of HP-NPs and NPs, and Tables II and III represent respective AUC values for the organs. Plasma profiles of DOX could not be measured for NPs and HP-NPs since the levels were below the detection limit of the assay for most of the plasma samples taken in a 48 h period. The whole liver was regarded as the liver tumor, because the hepatoma had spread by induction throughout the entire liver. HP-NPs exhibited the highest DOX profiles for the liver, while SOL exhibited the highest DOX profiles for the heart and other tissues in both normal and hepatoma-induced rats (Figs. 7 and 8, respectively).

The AUC of DOX was in the order of HP-NPs >>NPs >> SOL for the liver, HP-NPs<NPs<< SOL for the heart and lung, HP-NPs ≤NPs<< SOL for the spleen, and HP-NPs ≅ NPs ≅ SOL for the brain (Table II), with increased prominence in hepatoma rats (Table III). In the case of SOL, more distribution to the heart than to the liver was observed for both normal and hepatoma rats, consistent with well-known cardiotoxicity problems of conventional solution formulations of DOX (4).

The merit of HP-NPs over NPs and SOL in terms of DOX targeting efficiency and side effects may be described simply by introducing a concept of "merit index," which is defined as the AUC ratio of DOX in the liver (target organ) to DOX in the heart (an organ of major side effects). The index may represent not only targeting efficiency but also the safety margin of the formulation.

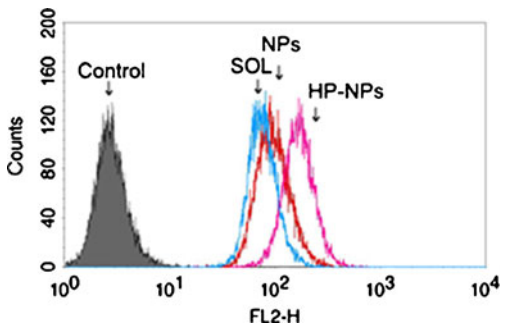

Fig. 4 FACS analysis of HepG2 cells after treatments with SOL, NPs and HP-NPs at 37°C for 6 h at DOX concentration of 170 μM. The control means plain medium without DOX.

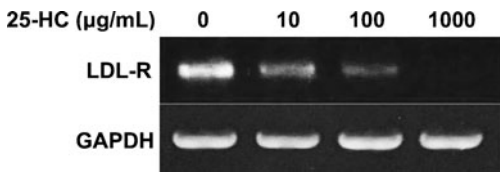

Fig. 5 RT-PCR products from HepG2 cells after treatments with 0, 10, 100 and 1000 μg/mL of 25-hydroxycholesterol (from *left* to *right*) for LDL R(LDL receptor gene) and GAPDH. Band intensities were normalized to the corresponding GAPDH intensity, which were regarded as 100%.

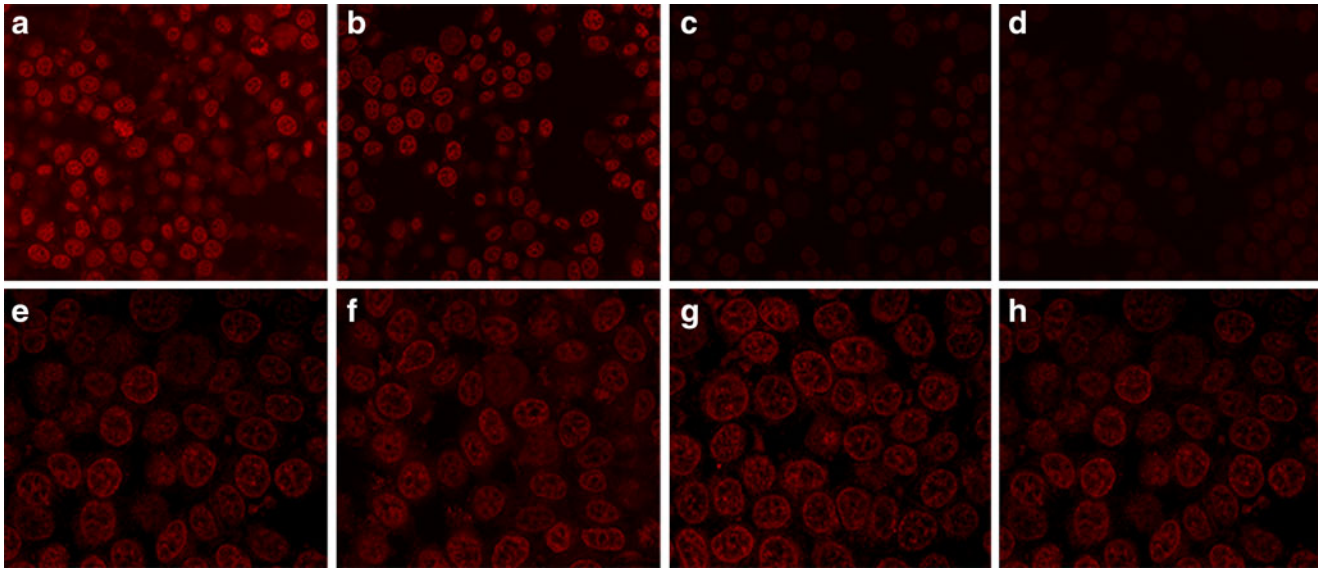

Fig. 6 Confocal images of HepG2 cells after the treatment with HP-NPs (**a–d**) and NPs (**e–h**) at 37°C for 6 h at DOX concentration of 170 μM following pretreatments of the cells with 0 (**a**, **e**), 10 (**b**, **f**), 100 (**c**, **g**) 1000 (**d**, **h**) μg/mL of 25-hydroxycholesterol for 48 h at 37°C to reduce the expression of LDL receptors.

In normal rats, the index was 58.1, 13.0 and 0.69 for HP-NPs, NPs and SOL, respectively, suggesting the merit of HP-NPs and NPs was 84.7 and 19.0 times greater, respectively, than SOL. In liver cancer-induced rats, the index was 45.3, 11.2 and 0.34 for HP-NPs, NPs, and SOL, respectively, suggesting the merit of HP-NPs and NPs was 132.5- and 32.7-times greater, respectively, than SOL. Particularly, the merit index of HP-NPs was more than 4-times greater than those of NPs in both normal and cancer rats.

Taken together, NPs and HP-NPs, particularly HP-NPs in cancer rats, demonstrated substantially greater merit over SOL, because DOX accumulated more in the liver (target organ) and less in the heart (an organ of major side effects) and other tissues (e.g., spleen and lung).

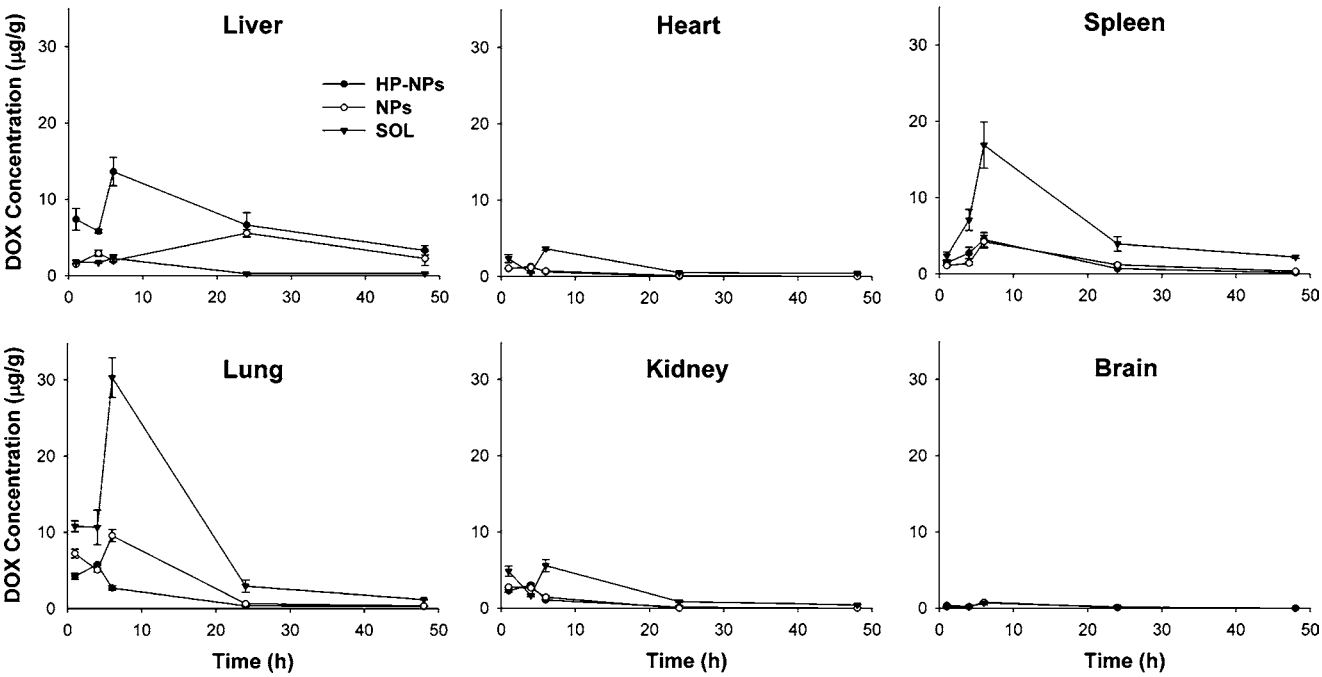

Fig. 7 Biodistribution of DOX in the tissues for SOL, NPs and HP-NPs in normal rats ($n = 3$). Each formulation was IV injected at a DOX dose of 2 mg/kg and the organs were excised at 1, 2, 4, 6, 12, 24, and 48 h after the injection.

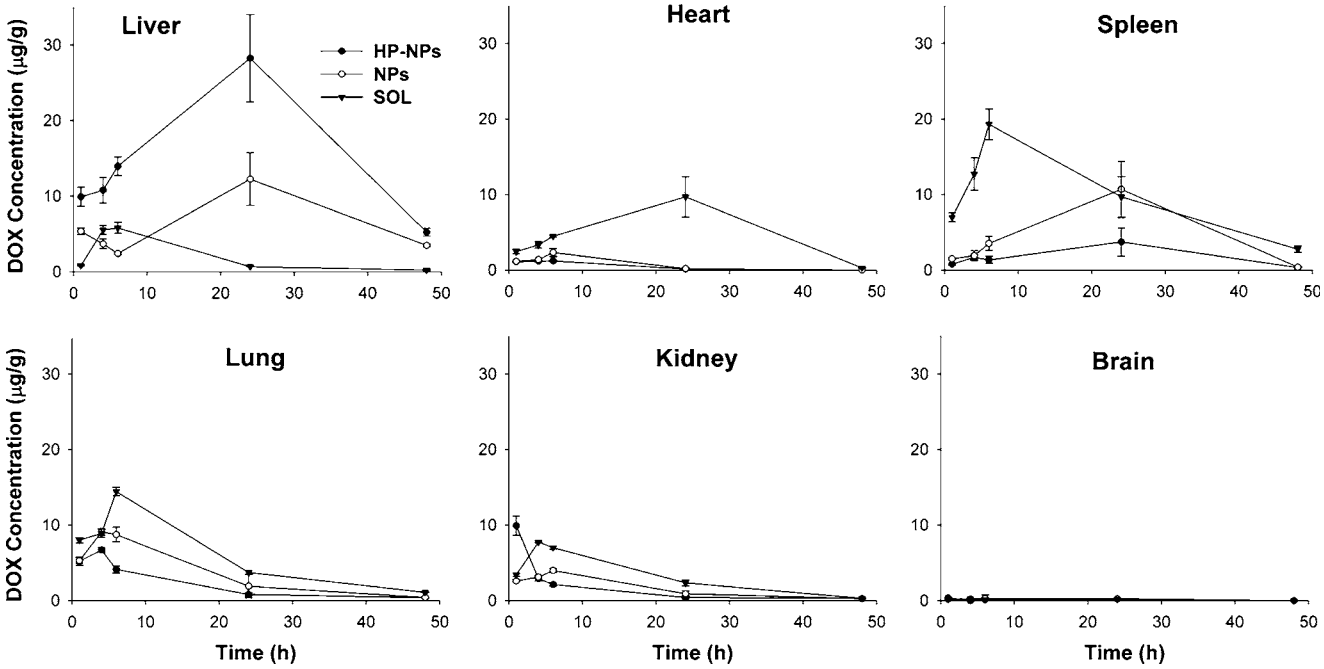

Fig. 8 Biodistribution of DOX in the tissues for SOL, NPs and HP-NPs in liver cancer-induced rats ($n=3$). Each formulation was IV injected at a DOX dose of 2 mg/kg and the organs were excised at 1, 2, 4, 6, 12, 24, and 48 h after the injection.

Safety and Anti-tumor Efficacy

In vivo safety and anti-tumor efficacy of PBS, SOL, NPs, and HP-NPs were assessed in hepatoma tumor-induced mice on days 0, 4, 8 and 12. As shown in Fig. 9a, significant weight loss was observed in SOL-treated mice, consistent with systemic toxicity of anti-cancer agents. However, weight loss was not observed for either NPs or HP-NPs, and instead, gradual weight gain was observed, suggesting improved safety of the nanoparticle formulations compared to SOL.

The tumor volume significantly increased over time in PBS-administered mice, while the increase was suppressed by the treatment with DOX-containing formulations, with the greatest suppression by HP-NPs, followed by NPs and SOL (Fig. 9b). For example, the tumor size on day 21 in SOL-treated mice was 1047.9 ± 113.7 mm^3 ($n=5$). Although the suppression of size increase was not significant in the case of NP treatment, the suppression by HP-NPs to 712.9 ± 80.6 mm^3 ($n=5$) was significant ($p<0.01$), suggesting a greater potency of HP-NPs compared to NPs and SOL in terms of efficacy (tumor suppression).

DISCUSSION

The present study examined the effects of surface modification with HP of NPs (i.e., DOX-loaded albumin nanoparticles) on targeted delivery of DOX to liver tumors. In the preparation of BSA nanoparticles, glutaraldehyde was used as a crosslinking agent. Considering the toxicity concerns of glutaraldehyde, however, replacement by safer substitutes may be necessary in the clinical development of BSA nanoparticles. The ideal size of nanoparticles for optimum uptake into tumor cells has not been determined precisely, but it is believed to be between 200 nm and 1.2 μm (35). The size of nanoparticles prepared in the present study was around 300 nm, consistent with the proposed range of 200 nm and 1.2 μm. The NPs were then modified with HP via conjugation with residual amino groups of BSA on the surface of the NPs. HP was selected because it acts as a ligand for LDL receptors (13), allowing for specific delivery of HP into tumors via the LDL receptors (36).

In vitro cell viability (Fig. 2) and cellular accumulation studies (Figs. 3 and 4) revealed enhanced accumulation of

Table II AUC Values of DOX for 48 h in the Tissues Following IV Administration of SOL, NPs, and HP-NPs to Normal Rats at a DOX dose of 2 mg/kg ($n=3$)

AUC(hr•μg/g)	Liver	Heart	Spleen	Lung	Kidney	Brain	Merit Index (Liver/Heart)
HP-NPs	344.0	5.92	71.1	61.2	24.1	9.8	58.1 (84.7-fold)
NPs	172.9	13.3	77.0	141.2	13.6	9.7	13.0 (19.0-fold)
SOL	39.5	57.6	300.3	427.0	93.0	9.1	0.69 (1)

Table III AUC Values of DOX for 48 h in the Tissues Following IV Administration of SOL, NPs, and HP-NPs to Liver Cancer-Induced Rats at a DOX Dose of 2 mg/kg ($n = 3$)

AUC (hr•μg/g)	Liver	Heart	Spleen	Lung	Kidney	Brain	Merit Index (Liver/Heart)
HP-NPs	842.9	18.6	101.4	90.5	60.7	4.1	45.3 (132.5-fold)
NPs	343.1	30.6	271.9	166.2	75.2	5.9	11.2 (32.7-fold)
SOL	90.6	265.4	475.0	274.2	149.3	4.2	0.34 (1)

DOX in HepG2 cells by HP-modified NPs. Considering that physical characteristics such as particle size, zeta potential, loading content, loading efficiency (Table I), and dissolution are comparable between NPs and HP-NPs, the enhancement appeared to be attributable to HP modification. Furthermore, since the accumulation of DOX is greatly associated with LDL receptors (Figs. 5 and 6), it was suggested that HP moiety on the surface of HP-NPs might have bound to LDL receptors on HepG2 cells, thereby accelerating DOX uptake probably via a receptor-mediated endocytosis (RME) mechanism.

Following iv administration to rats, nanoparticles, particularly HP-NPs, greatly increased the distribution of DOX to the liver, along with greatly decreased distribution to the heart, compared to unmodified NPs and SOL, particularly in hepatoma rats (Figs. 7 and 8). Following the administration of NPs and HP-NPs, plasma concentrations of DOX were below the detection limit of the assay, probably due to substantial distribution of DOX to other organs including the liver. This was consistent with the result that nanoparticles, compared to solution dosage forms, were likely to accumulate more in the liver, a major reticuloendothelial system (RES) organ, via a passive mechanism (37). Enhanced permeability and retention (EPR) due to the immature and porous vasculature of tumors (38) might have increased the uptake of nanoparticles in the liver of hepatoma rats. Considering the *in vitro* results (Figs. 5 and 6) together with the fact that many tumors show relatively elevated levels of LDL receptors (39), a greater accumulation of DOX in the hepatoma-induced liver by HP-modifiied nanoparticles appears to be associated with LDL receptor-mediated endocytosis of nanoparticles by both by hepatocytes and hepatoma cells. The uptake by Kupffer cells, which express LDL receptors (40), might have contributed, if any, to the hepatic distribution of DOX.

The AUC of DOX in the liver was much greater for NPs and HP-NPs compared to SOL, while the AUC in the heart was much smaller compared to SOL (Tables II and III). In the case of SOL, more distribution to the heart than to the liver was observed for both normal and hepatoma rats, consistent with cardiotoxicity problems of conventional solution formulations of DOX (4). The merit index (i.e., the AUC ratio of DOX in the liver to DOX in the heart) of HP-NPs was 84.7- and 4.5-times greater in normal rats, and 132.5- and 4.0-times greater in hepatoma rats, than those of SOL and NPs, respectively. This indicated that HP-modified nanoparticles (e.g., HP-NPs) have substantial advantages not only over SOL but also over NPs in terms of specific delivery of DOX to the liver with much less accumulation in the heart. This means that not only the anti-tumor efficacy of DOX would be maximized, but also the cardiotoxicity problems of DOX would be substantially reduced when the drug is administered in the form of

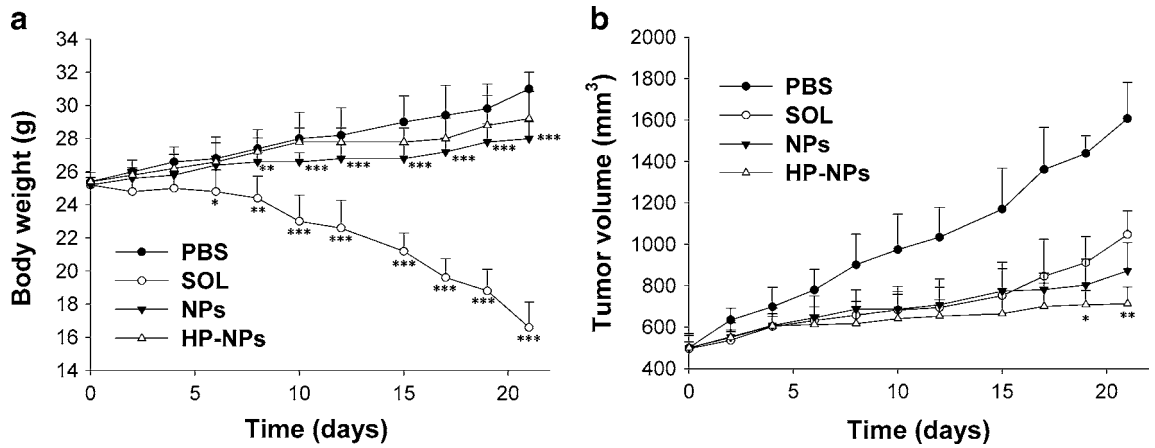

Fig. 9 Changes in the body weight (**a**) and the tumor size (**b**) of nude mice bearing a hepatoma tumor following IV injection of PBS, SOL, NPs and HP-NPs at a DOX dose of 2 mg/kg (n = 5). Each formulation was injected 4 times at a 4-day interval (Day 0, 4, 8, and 12) and the tumor size and body weight were monitored for 3 weeks. * $p < 0.5$, ** $p < 0.01$, *** $p < 0.001$, compared with PBS (**a**) and SOL (**b**).

HP-NPs. However, the potential toxicity of DOX to normal hepatocytes, as well as the anti-tumor efficacy to hepatoma cells, might also be increased in the case of HP-NPs, when the DOX dose is identical to SOL. In such cases, the administration of smaller dose of the drug would reduce the hepatotoxicity problem. In fact, the dose of DOX that is needed to show equal anti-tumor efficacy is expected to be in the order of HP-NPs <NPs<<SOL based on the merit index.

Consistent with the results in Tables II and III, the greatest increase in body weight together with the least increase in tumor volume was observed for HP-NPs, followed by NPs and SOL (Fig. 9). The body weight increase appears to be associated with the suppression of the tumor-related toxicity.

CONCLUSIONS

HP modification of the surface of DOX-loaded BSA nanoparticles significantly enhanced the delivery of DOX to liver tumors in rats, and reduced the distribution to the heart, a major side effect organ of DOX, demonstrating the usefulness of the surface-modification of nanoparticles (passive carrier) with ligands for cancer cell-specific receptors in the delivery of anticancer drugs to tumors. The HP moiety might have contributed to the binding of BSA nanoparticles to LDL receptors on the liver cancer cells resulting in accelerated uptake of NPs possibly via an active transport mechanism of RME.

ACKNOWLEDGMENTS & DISCLOSURES

This work was supported by a grant from the Korean Ministry of Science and Technology through the National Research Laboratory Program (Grant Number ROA-2006-000-10290-0).

REFERENCES

1. Olweny C, Toya T, Katongole-Mbidde E, Mugerwa J, Kyalwazi S, Cohen H. Treatment of hepatocellular carcinoma with adriamycin. Preliminary communication. Cancer. 1975;36:1250–7.
2. Yang T, Wang C, Hsieh R, Chen J, Fung M. Gemcitabine and doxorubicin for the treatment of patients with advanced hepatocellular carcinoma: a phase I-II trial. Ann Oncol. 2002;13:1771–8.
3. Park J, Fong P, Lu J, Russell K, Booth C, Saltzman W, *et al.* PEGylated PLGA nanoparticles for the improved delivery of doxorubicin. Nanomed Nanotechnol Biol Med. 2009;5:410–8.
4. Li C. Poly (-glutamic acid)-anticancer drug conjugates. Adv Drug Deliv Rev. 2002;54:695–713.
5. Maeng J, Lee D, Jung K, Bae Y, Park I, Jeong S, *et al.* Multifunctional doxorubicin loaded superparamagnetic iron oxide nanoparticles for chemotherapy and magnetic resonance imaging in liver cancer. Biomaterials. 2010;31:4995–5006.
6. Gieseler F, Rudolph P, Kloeppel G, Foelsch U. Resistance mechanisms of gastrointestinal cancers: why does conventional chemotherapy fail? Int J Colorectal Dis. 2003;18:470–80.
7. Brigger I, Dubernet C, Couvreur P. Nanoparticles in cancer therapy and diagnosis. Adv Drug Deliv Rev. 2002;54:631–51.
8. Na K, Lee B. Self-assembled nanoparticles of hydrophobically-modified polysaccharide bearing vitamin H as a targeted anti-cancer drug delivery system. Eur J Pharm Sci. 2003;18:165–73.
9. Brannon-Peppas L, Blanchette J. Nanoparticle and targeted systems for cancer therapy. Adv Drug Deliv Rev. 2004;56:1649–59.
10. Xu Z, Chen L, Gu W, Gao Y, Lin L, Zhang Z, *et al.* The performance of docetaxel-loaded solid lipid nanoparticles targeted to hepatocellular carcinoma. Biomaterials. 2009;30:226–32.
11. Green M, Manikhas G, Orlov S, Afanasyev B, Makhson A, Bhar P, *et al.* Abraxane®, a novel Cremophor®-free, albumin-bound particle form of paclitaxel for the treatment of advanced non-small-cell lung cancer. Ann Oncol. 2006;17:1263–8.
12. Liang H, Chen C, Chen S, Kulkarni A, Chiu Y, Chen M, *et al.* Paclitaxel-loaded poly (γ-glutamic acid)-poly (lactide) nanoparticles as a targeted drug delivery system for the treatment of liver cancer. Biomaterials. 2006;27:2051–9.
13. Berg K, Selbo P, Weyergang A, Dietze A, Prasmickaite L, Bonsted A, *et al.* Porphyrin related photosensitizers for cancer imaging and therapeutic applications. J Microsc. 2005;218:133–47.
14. Isakau H, Parkhats M, Knyukshto V, Dzhagarov B, Petrov E, Petrov P. Toward understanding the high PDT efficacy of chlorin e6-polyvinylpyrrolidone formulations: Photophysical and molecular aspects of photosensitizer-polymer interaction *in vitro*. J Photochem Photobiol B Biol. 2008;92:165–74.
15. Yang S, Chang J, Shin B, Park S, Na K, Shim C. 99mTc-hematoporphyrin linked albumin nanoparticles for lung cancer targeted photodynamic therapy and imaging. J Mater Chem. 2010;20:9042–6.
16. Dreis S, Rothweiler F, Michaelis M, Cinatl J, Kreuter J, Langer K. Preparation, characterisation and maintenance of drug efficacy of doxorubicin-loaded human serum albumin (HSA) nanoparticles. Int J Pharm. 2007;341:207–14.
17. Weber C, Kreuter J, Langer K. Desolvation process and surface characteristics of HSA-nanoparticles. Int J Pharm. 2000;196:197–200.
18. Hamblin M, Newman E. Photosensitizer targeting in photodynamic therapy I. Conjugates of haematoporphyrin with albumin and transferrin. J Photochem Photobiol B Biol. 1994;26:45–56.
19. Nam Y, Kang H, Park J, Park T, Han S, Chang I. New micelle-like polymer aggregates made from PEI-PLGA diblock copolymers: micellar characteristics and cellular uptake. Biomaterials. 2003;24:2053–9.
20. Weber C, Coester C, Kreuter J, Langer K. Desolvation process and surface characterisation of protein nanoparticles. Int J Pharm. 2000;194:91–102.
21. Lim S, Kim C. Formulation parameters determining the physicochemical characteristics of solid lipid nanoparticles loaded with all-trans retinoic acid. Int J Pharm. 2002;243:135–46.
22. Merodio M, Arnedo A, Renedo M, Irache J. Ganciclovir-loaded albumin nanoparticles: characterization and *in vitro* release properties. Eur J Pharm Sci. 2001;12:251–9.
23. Zhou Q, Chowbay B. Determination of doxorubicin and its metabolites in rat serum and bile by LC: application to preclinical pharmacokinetic studies. J Pharm Biomed Anal. 2002;30:1063–74.
24. Mu L, Feng S. A novel controlled release formulation for the anticancer drug paclitaxel (Taxol®): PLGA nanoparticles containing vitamin E TPGS. J Control Release. 2003;86:33–48.

25. Yoo H, Lee K, Oh J, Park T. *In vitro* and *in vivo* anti-tumor activities of nanoparticles based on doxorubicin-PLGA conjugates. J Control Release. 2000;68:419–31.
26. Janes K, Fresneau M, Marazuela A, Fabra A, Alonso M. Chitosan nanoparticles as delivery systems for doxorubicin. J Control Release. 2001;73:255–67.
27. Yoo H, Park T. Biodegradable polymeric micelles composed of doxorubicin conjugated PLGA-PEG block copolymer. J Control Release. 2001;70:63–70.
28. Panyam J, Zhou W, Prabha S, Sahoo S, Labhasetwar V. Rapid endo-lysosomal escape of poly (DL-lactide-co-glycolide) nanoparticles: implications for drug and gene delivery. FASEB J. 2002;16:1217–26.
29. Lin W, Tsai S, Hsieh J, Wang S. Effects of 90Y-microspheres on liver tumors: comparison of intratumoral injection method and intra-arterial injection method. J Nucl Med. 2000;41:1892–7.
30. Jaroszeski M, Gilbert R, Heller R. *In vivo* antitumor effects of electrochemotherapy in a hepatoma model. Biochim Biophys Acta-General Subjects. 1997;1334:15–8.
31. Han Y, Chung S, Shim C. Canalicular membrane transport is primarily responsible for the difference in hepatobiliary excretion of triethylmethylammonium and tributylmethylammonium in rats. Drug Metab Dispos. 1999;27:872–9.
32. Vos T, Caracoti A, Che J, Dai M, Farrer C, Forsyth N, *et al.* Identification of 2-{2-(2-(5-bromo-2-methoxyphenyl)-ethyl)-3-fluorophenyl}-4, 5-dihydro-1H-imidazole (ML00253764), a small molecule melanocortin 4 receptor antagonist that effectively reduces tumor-induced weight loss in a mouse model. J Med Chem. 2004;47:1602–4.
33. Allison B, Pritchard P, Levy J. Evidence for low-density lipoprotein receptor-mediated uptake of benzoporphyrin derivative. Br J Cancer. 1994;69:833–9.
34. Srivastava R, Ito H, Hess M, Srivastava N, Schonfeld G. Regulation of low density lipoprotein receptor gene expression in HepG2 and Caco2 cells by palmitate, oleate, and 25-hydroxycholesterol. J Lipid Res. 1995;36:1434–46.
35. Hobbs SK, Monsky WL, Yuan F, Roberts WG, Griffith L, Torchilin VP, *et al.* Regulation of transport pathways in tumor vessels: role of tumor type and microenvironment. Proc Natl Acad Sci USA. 1998;95:4607–12.
36. Barel A, Jori G, Perin A, Romandini P, Pagnan A, Biffanti S. Role of high-, low-and very low-density lipoproteins in the transport and tumor-delivery of hematoporphyrin *in vivo*. Cancer Lett. 1986;32:145–50.
37. Yi Y, Kim JH, Kang HW, Oh HS, Kim SW, Seo MH. A polymeric nanoparticle consisting of mPEG-PLA-Toco and PLMA-COONa as a drug carrier: improvements in cellular uptake and biodistribution. Pharm Res. 2005;22:200–8.
38. Gao ZG, Tian L, Hu J, Park IS, Bae YH. Prevention of metastasis in a 4T1 murine breast cancer model by doxorubicin carried by folate conjugated pH sensitive polymeric micelles. J Control Release. 2011;152:84–9.
39. Firestone RA. Low-density lipoprotein as a vehicle for targeting antitumor compounds to cancer cells. Bioconjug Chem. 1994;5:105–13.
40. Kamps J, Kruijt JK, Kuiper J, Van Berkel T. Uptake and degradation of human low-density lipoprotein by human liver parenchymal and Kupffer cells in culture. Biochem J. 1991;276:135–40.